DE9

properties as coatings but the oxides that they produce are non-stoich

case there is always a finite rate of diffusion to the interface and oxidati

Consequently the films are mechanically unstable and tend to dete

perhaps, in either case, be more precise to speak of 'metal oxide' coatin

CONF-9005145--1

The Theory and Practice of

High Resolution Scanning Electron Microscopy

CONF-9005145--1

DE91 000718

David C Joy

EM Facility and Dept. of Zoology, University of Tennessee

Knoxville, TN 37996-0810

and

Metals and Ceramics Division, Oak Ridge National Laboratory+

Oak Ridge, TN 37831

Abstract

Recent advances in instrumentation have produced the first commercial examples of what can justifiably be called High Resolution Scanning Electron Microscopes. The key components of such instruments are a cold field emission gun, a small-gap immersion probe-forming lens, and a clean dry-pumped vacuum. The performance of these microscopes is characterized by several major features including a spatial resolution, in secondary electron mode on solid specimens, which can exceed 1nm on a routine basis; an incident probe current density of the order of 10^6 amps/cm^2; and the ability to maintain these levels of performance over an accelerating voltage range of from 1 to 30keV. This combination of high resolution, high probe current, low contamination and and flexible electron-optical conditions provides many new opportunities for the application of the SEM to materials science, physics, and the life sciences.

+Operated by Martin Marietta Energy Systems, Inc., under contract DE-AC05-84OR21400 with the U.S. Department of Energy.

"The submitted manuscript has been authored by a contractor of the U.S. Government under contract No. DE-AC05-84OR21400. Accordingly, the U.S. Government retains a nonexclusive, royalty-free license to publish or reproduce the published form of this contribution, or allow others to do so, for U.S. Government purposes."

MASTER

DISTRIBUTION OF THIS DOCUMENT IS UNLIMITED

Introduction

Since its commercial introduction in the early 1960s the scanning electron microscope (SEM) has become widely used and appreciated for such features as its ease of operation, its relaxed requirements for specimen preparation, its striking three dimensional views of complex surfaces, and its excellent depth of field. It has not, however, become equally celebrated for its resolution which is typically viewed as being somewhat better than that of an optical microscope but significantly lower than that of a transmission electron microscope (TEM). This apparent restriction on the performance has been attributed both to fundamental limitations in the nature of the image forming process of the SEM and to the quality of the electron-optical components in the instrument. In the past two or three years, however, instruments which can reasonably be called 'High Resolution' Scanning Electron Microscopes have become commercially available. These machines combine the desirable features of the conventional SEM, including the use of solid specimens, with a level of spatial resolution which approaches (and sometimes matches) that available from a TEM. In addition they are able to maintain this level of performance over a wide range of incident electron energies, making it possible to choose the beam energy so as to optimize a particular contrast effect or interaction without penalty of resolution. This paper discusses the improvements in electron optics and in our understanding of electron-solid interactions which have facilitated these advances.

Instrumental Considerations

The purpose of the optical components in an SEM is to form a focussed, demagnified, image of the electron source at the plane of the specimen. The spatial resolution and signal to noise ratio of the image are ultimately limited by the size of the electron probe and by the amount of current which it contains, so it is in these two areas therefore that the performance of the system must be optimized. Common to all current high performance SEMs are two specific electron-optical components:

(1) A field emission electron source

The field emission gun (FEG) is the preferred electron source for several reasons. Firstly, the SEM is - under all imaging conditions - brightness limited. Because the image is sequentially acquired the recording time per pixel of the image is typically only a few microseconds. After allowing for the efficiencies of signal production within the specimen (e.g secondary electron yields are typically 0.03 to 0.1 per incident electron, backscatter electron yields range from 0.05 to 0.5), and for the geometrical efficiencies of the detector system (e.g ranging from 0.5 for a secondary electron detector to 0.05 for a backscatter detector), it is clear that even large incident beam currents will only result in a small number of detected electrons per pixel. Because electron optical brightness β is conserved, it follows that, in the absence of any optical aberrations, the current density is constant, hence the current in the incident beam falls as the square of the diameter of the electron probe. Since a high spatial resolution in the image requires a correspondingly small probe diameter, the current in the beam, and thus the signal to noise ratio of the image, inevitably degrades under high resolution conditions. The maximum current available at a given probe size depends directly on the brightness of the electron source. Since an FEG has a brightness which is of the order of 10^8 - 10^9 amps/cm^2/str at 20keV depending on the emission current into the tip, as compared to 10^6 amps/cm^2/str for an advanced thermionic emitter such as an LaB_6 cathode, the available imaging current is correspondingly increased. Secondly, the FEG has a small source size, usually in the range from 5 to 25 nm. The optics required to demagnify this probe to a value (0.5 to 1.5nm) suitable for high resolution operation are therefore considerably simplified compared to the case for a thermionic emitter where the effective source size is of the order of 5μm or more. Finally, the FEG has a low chromatic energy spread ΔE, varying from 0.15eV full width half maximum for a cold FEG to about 0.5eV for a thermal or Schottky FEG as compared to 1.5eV or more for a thermionic emitter and, as discussed below, while chromatic aberration is not a limitation in probe forming at high beam energies (>10keV) it is a major factor at low energies.

(2) A high excitation, short working distance, lens.

The role of the probe forming lens is to take the image of the electron source and to generate from it the final demagnified probe at the surface of the specimen. The quality of this probe will depend on the performance of the lens. Conventional SEMs were constrained by certain historical

requirements and beliefs - particularly the desire to use large samples, the goal of minimizing magnetic field penetration into the specimen chamber, and the need to place a variety of detectors around and above the sample - to a design in which the focal length of the lens was of the order of a centimeter or more. Since the spherical and chromatic aberrations of a lens scale with its focal length the limiting aberrations of the conventional SEM lens were of necessity large by the standards of the objective lens in a TEM. In the high performance SEM, on the other hand, the sample is placed within the lens at one of the positions where a crossover (i.e a focussed probe) can be formed. In this mode the focal length of the lens is of the order of 2mm, compared with 2cm for the older SEM, and the aberrations are thus also reduced by a corresponding factor. While placing the sample inside the lens severely restricts its size there are as compensation, in addition to the electron-optical benefits, significant gains in the electromagnetic shielding of the sample and in the physical stability of the specimen relative to the lens which also contribute to a marked improvement in performance. The current high performance SEMs available, e.g the Hitachi S900 and the JEOL JSM890, are essentially built around the objective lens portion of a high resolution TEM column, for example the Hitachi H7000, to which is added the field emission gun, additional electromagnetic screening, and a suitable UHV differential pumping system. Following Kimura and Tamura [1] it is also now standard to use the lens field to collect and guide the secondary electrons on to a detector placed just before the probe forming lens. This arrangement gives a high collection efficiency (>50%) without occupying any of the limited space in the lens gap, and also minimizes the collection of spurious secondary electrons produced by the impact of backscattered electrons or scattered primary electrons on the lens and chamber walls.

Optimizing electron-optical performance

The way in which the properties of the FEG and of the probe forming lens are coupled together depends on the operating energy of the instrument. At high beam energies the optimum operating condition of the instrument is that which produces the maximum beam current i_{max} into a probe of given diameter d. In this regime the performance is limited by the spherical aberration coefficient C_s of the lens and by the source brightness β and a straightforward calculation [2] shows the relationship between i_{max} and d to be:

$$d = (C_s^{1/4} \lambda^{3/4}) \left\{ \frac{i_{max}}{\beta \lambda^2} + 1 \right\}^{3/8} \qquad (1)$$

where λ is the electron wavelength and the beam convergence angle α is assumed to be maintained at the value $\alpha = (d/C_s)^{1/3}$. Figure (1) plots this relation for three typical SEM configurations, a conventional SEM with a tungsten hairpin thermionic emitter and a pinhole-lens (C_s = 2cm, $\beta = 10^5$ amps/cm^2/str), an SEM with conventional optics but using a field emission gun (C_s = 2cm, $\beta = 10^8$ amps/cm^2/str), and a high performance SEM with both a field emission gun and an immersion lens (C_s = 2mm, $\beta = 10^9$ amps/cm^2/str). It is evident that the high performance system provides both a smaller ultimate probe (although the minimum size varies only as $C_s^{1/4}$) and a higher usable current (which increases proportional to $C_s^{-2/3}$).

At low beam energies (<10keV) both diffraction and chromatic aberration effects must be considered in addition to spherical aberration when optimizing the optics. In this case quadrature addition of the aberration terms is not valid and a more sophisticated procedure, such as the numerical ray tracing method of Cliff and Kenway [3], must be used to optimize the electron-optical parameters. Such an analysis shows that the effect of chromatic aberration is usually dominant. Figure (2) shows a simulation, modeled by a modification of the Cliff and Kenway procedure, of the probe forming optics of an SEM with an immersion type lens (C_s=2mm) but using either a LaB_6 or an FEG electron source. At 30keV both sources produce probes of essentially identical size, the only difference being the current in the probe. At 2keV, however, it can be seen that while the FEG source maintains the size and quality of the probe, the LaB_6 source produces a probe which is not only significant broader but which is also non-Gaussian in form due to the presence of a chromatic skirt region extending to two or three times the nominal FWHM resolution of the probe. The effect of this chromatic skirt, which becomes even more severe at lower beam energies, is to transfer current from the center to the edge of the probe, and so reduce both contrast and signal to noise in the image. High performance at low beam energies thus demands both an FEG and a good lens.

As a consequence of the use of an immersion lens, the depth of field d_f of a high resolution SEM, defined [2] from the equation

$$d_f = \frac{\text{pixel size}}{\alpha} \qquad (2)$$

is relatively small compared to that found in a conventional SEM because α, the numerical aperture of the lens (whose optimum size varies as $C_s^{-1/3}$), is large and because operation at high magnifications also results in a small pixel size for the image display. Thus the habit, common in normal SEM operation, of placing the sample at a tilt (30 or 45 degrees) to improve the secondary yield is not particularly helpful in the high performance SEM since the restricted depth of field will limit the usable field of view to just the central portion of the display. The limited depth of field also greatly increases the importance of accurate focus and astigmatism correction and high resolution SEMs are therefore usually fitted with special 'fine' adjustments for this purpose.

There is, at present, no widely accepted procedure for quantitatively assessing the electron-optical performance of a high performance SEM. While estimates of the resolution obtained from measurements of selected images have anecdotal interest they are of little comparative value because they are highly sample dependent. An acceptable procedure for defining performance would be one which gives a measurement of the resolution achieved, and some indication of the signal to noise ratio at the specified operating condition, without relying on the properties of a specific sample. In the TEM the corresponding measurement is made by observing the transfer function of the image of a thin phase object assumed to have a fully random 'white-noise' structure to a limit beyond the resolution of the instrument. For scanning electron microscopy no object with correspondingly ideal properties has yet been suggested, but two-dimensional Fourier transforms of secondary electron images of very fine grain (<1nm diameter) metal dispersions [4] do seem to show that available detail is transferred to a resolution of about 1.2 to 1.5nm before fading into the noise of the recording system. More work in this area is required to make it possible to measure, and hence optimize and finally compare, the performance of these systems in an objective and convenient manner.

Image formation and interpretation in high resolution SEM

Two basic modes of signal generation, secondary electron and backscattered electron imaging, account for the majority of the use of the SEM. The properties and limitations of these modes will now be briefly considered in the context of high resolution operation.

(1)Secondary Electron Imaging

(a) Principles

Secondary electrons (SEs) are defined as those electrons emitted from the specimen with energies of from zero to 50eV. These SEs are generated within the sample by a variety of mechanisms [5] associated with the passage of high energy electrons through the specimen Typically the SEs which leave the specimen are the end product of a cascade process in which an initial single secondary electron of relatively high energy (50-100eV) transfers some of its energy to a low energy electron to form a pair of SEs each with about half or less of the original energy, each of this pair then in turn generates a further pair of SE of still lower energy and so on until the average energy of the cascade falls to a value at which there is no longer any inelastic process of sufficiently large cross-section for further multiplication to occur. The cascade then diffuses through the sample, suffering mostly elastic scattering events, until the SEs are either thermalized or, if they have approached the surface potential barrier at a suitable angle and with sufficient energy, escape to the vacuum. The maximum distance between the initiation point of a cascade and the eventual escape through the surface of an SE , although larger than popularly supposed, is only of the order of 5 to 15nm in most materials.

In general, (figure 3), there are only two conditions when SE produced by an electron can escape from the specimen and contribute to the collected image: when the SE is generated close to the surface by an incident primary electron and when the SE is generated by a backscattered electron as it leaves the surface. In the first case as the beam passes down through the first five to ten nanometers of material below the surface, SEs generated along the track of the incident electron will be able to escape. These secondaries, usually called SE1 electrons [6], should contain the highest resolution information about the sample since they come from the immediate vicinity of the

beam impact point. Monte Carlo simulations [7] show that the SE1 electrons from a material such as aluminum leave the surface with a Gaussian intensity profile which has a full width at half maximum intensity (FWHM) of about 2nm. As the beam travels into the target secondaries will, of course, continue to be generated but they will not escape to the surface and be detected.

If the electron is backscattered then it once more passes through the region immediately below the surface and the secondaries that it produces can again reach the surface and be collected. This component of the signal, usually referred to as the SE2 electrons, leaves the surface with an intensity profile that is again Gaussian but now with a FWHM that is typically of the order of 0.2 to 0.4 of the Bethe range R_B of the incident electrons where [2] R_B can be approximated as :

$$R_B = 76.\frac{E^{1.66}}{\rho} \quad \text{(nm)} \qquad (3)$$

E is the energy of the incident electrons in keV and ρ is the density of the target in gm/cc. The overall intensity distribution of SE production from the surface thus has the appearance shown schematically in figure 4. The information carried by the SE2 signal depends both on the number and the average energy of the electrons backscattered from the incident beam, and the way in which these backscattered electrons interact with the surfaces through which they pass as they leave the specimen . The SE2 signal is thus complex to interpret since it is affected by the details of the specimen at points remote from the incident beam.

The total emitted secondary yield, δ_{SE} is given as

$$\delta_{SE} = \delta_{SE1} + \delta_{SE2} = \delta_{SE1}(1 + \kappa\eta) \qquad (4)$$

since for each incident electron there are η backscattered electrons (where η is the backscatter yield) each of which produces secondary electrons with a relative efficiency κ. Because the backscattered electrons are lower in energy than the incident electrons, and because they approach the surface over a range of angles, κ is typically between 2 and 4 [5,8] at all incident beam

energies, so the SE1 component varies from as much as 80% of the total for carbon (for which η=0.06) to as low as 30% for gold (for which η=0.5). The SE1 and SE2 signal components cannot be separated from one another by any physical means since they have identical emitted energy and angular distributions. So apart from the limiting case where the sample is sufficiently electron transparent that there is no backscattering and the SE2 component is zero [9], procedures to generate high resolution secondary electron images must involve some method for minimizing the unwanted effects of the low resolution SE2 component.

One situation in which some discrimination of the SE1 component can be achieved is obtained at high beam energies. Consider for example a beam of energy 30keV incident on a sample of silicon. The SE1 component of the secondary signal (the 'spike' of figure 4) will have a width of 2nm or so, but the SE2 component will be emerging from the surface over a diameter of about 4 - 5μm about the beam point. If the sample is scanned at a low magnification, say x10,000, then the field of view of the image is of the order of 10μm and as the beam moves from point to point within this field the SE2 component can be expected to change and contribute to the signal contrast. If, however, the sample is scanned at magnification of x250,000 then the field of view is only 0.4μm, a value which is small compared with the SE2 interaction volume. We can predict in this case that scanning the beam across this field of view will not significantly change the SE2 signal so all of the contrast (i.e point to point variation) in the signal will therefore be due to the SE1 component. Although the SE2 component has not been removed the fact that it is constant means that its effect on the image has been minimized and consequently the task of interpreting the image has been simplified. Figure (5) shows an image recorded in this way from a specimen of anodized alumina used as an inorganic membrane. The material , which was fractured in liquid nitrogen to reveal both the plan and the cross-sectional views of the microstructure, was uncoated but no charging problems were encountered because the high beam energy ensured that the majority of the beam energy is deposited in the silicon substrate rather than in the oxide. Although the form of the image looks very like that observed at lower magnifications and resolutions, care is necessary in interpreting the image and, as for high resolution TEM studies, image simulation methods are an appropriate tool [10].

A second approach relies on the fact that, while the SE1 distribution is constant in size, the SE2 interaction volume (as shown by equation 3) varies rapidly with beam energy. For beam energies of a few keV, equation (3) shows that the SE1 and SE2 signals are coming from volumes of the same size. Because there is no longer a spatial distinction between the SE1 and SE2 signals, both will contribute contrast information at high resolution to the secondary image. This is clearly a favorable situation since all, rather than just 50% or less, of the signal is now carrying useful contrast. In addition because the secondary yield rises as the beam energy falls, then the total amount of signal available increases. The drawback to operating in this condition is that it requires the use of beam energies which, even on a high performance SEM, are low enough that the performance of the optics is beginning to degrade in comparison to the probe diameter and beam currents available at higher energies. Operation at low beam energy is also more susceptible to problems with contamination and charging, but if these practical problems can be adequately overcome then low voltage microscopy is perhaps the optimum arrangement. Figure (6) shows an image of a layerered Si-Ge semiconductor structure imaged in this mode. The layers with a spacing of 10nm are easily resolved and display a small amount of contrast associated with their different chemical composition (Si is dark and Ge is bright). By comparison with the lengthy process required to obtain a similar view of this structure in the TEM the only preparation required here was to fracture the sample in liquid nitrogen and face the edge of interest towards the beam. The field of view that can be examined is also, of course, much greater in the SEM.

(b) Information in the SE image

The information carried by the SE signal remains the same under most operating conditions although the details may vary depending on the magnification of the image. The yields of the SE1 and SE2 components vary with the angle of incidence of the beam to the surface, so both can carry contrast related to the topography of the specimen. If the topography is on a scale commensurate with the SE2 interaction volume (i.e 50nm and above) then the surface details will be visible in the low and medium magnification images in which the SE2 component dominates but the high magnification image (SE1 component) may be relatively featureless. If the topography is on a very fine scale then at low and medium magnifications the surface structure may not be resolved although the surface will appear to be 'bright' because of an enhanced secondary yield.

The surface structure will, however, be visible at high magnification where the SE1 signal contributes most to the displayed contrast.

The secondary yield will also, in principle, reflect the chemical nature of the specimen. At low magnifications, changes in the mean atomic number Z of the target will change the backscattering yield (which is almost linearly proportional to Z) and hence vary the SE2 component of the signal. The SE1 yield is also, as shown in the Monte Carlo calculations of figure (7), dependent on the atomic number [11] being larger for the highest atomic number and most dense materials. In practice the surfaces of specimens being examined are often covered with a sufficient thickness (5-10nm) of low atomic number contaminant that these atomic number dependent effects are masked.

Both SE components also exhibit 'edge' contrast which arises when the incident beam is placed close to an edge the sample. In this case there are two possible escape paths for the secondaries, one through the entrance surface of the specimen and another through the side surface at the edge. Because of the SE2 contribution to low and medium magnification micrographs this effect is familiar in the standard SEM. Every edge in the secondary image is highlighted by a bright line whose maximum intensity is about twice the nominal secondary signal level and which has a width of about $R_B/2$, i.e typically fractions of a micron. This contrast effect also occurs in the SE1 image although, in this case, the width of the bright line is determined by the probe size and the FWHM of the SE1 emission profile and is typically only 2-3nm in extent. A measurement of the width of the SE1 bright line along a suitable edge is, in fact, one of the best ways of routinely checking the resolution of a high performance SEM.

(c) Limits of SE imaging

For low atomic number, low density, materials such as soft biological tissue, or polymers, the utility of SE imaging is ultimately limited by two effects. Firstly, as the incident probe size is decreased the current in the probe falls (figure 1) until eventually it is below the threshold value [2] required for satisfactory imaging. The magnitude of the threshold current depends on the nature of the specimen, the beam energy, and other experimental variables, but it is typically of the order of

5 - 10 pA for a low atomic number material observed at a beam energy of 30keV. Secondly we encounter (figure 8) what could be called the classical limit of secondary electron imaging. As discussed above each feature in the image will show SE1 bright line contrast along each edge (fig 8a). When the edges are spaced 20 or 30nm apart then the bright lines are well separated and the true shape of the feature will be delineated. But as the feature size is made smaller (fig 8b) then bright line start to overlap until eventually (fig 8c) for a feature size of a 4-5 nm in the case of a low density material they overlap. In this limiting condition the feature is not resolved, but simply appears as a bright dot of indeterminate size and shape, an effect often referred to as 'particle contrast'. Figure 9(a), which shows an image of a polystyrene sphere to which are bound strands of monoclonal anti-body protein, illustrates both of these problems. The poor signal to noise ratio of the image is evident both in the graininess of the micrograph and by the fact that protein strands are visible only at the edge of the sphere where, because the beam is almost at a glancing angle of incidence to the surface, the contrast and signal are highest. The resolution limit is demonstrated by the fact that the 4-5nm wide protein strands appear only as diffuse bright lines with no defined edges or shape.

Some relief from both of these problems can be obtained by the careful use of metal films. The first purpose of the coating is to increase the SE1 yield, so as to give a higher signal to noise ratio in the image. As shown by the data of figure (7) the SE1 yield of almost any metal is significantly greater than that from the carbon matrix of a biological or polymeric specimen. Since, however, it is desirable that the coating film not contribute any structure of its own to the image some obvious candidates for coating materials, such as gold, must be eliminated from consideration since at suitable thicknesses they cannot form a continuous layer. Transition metals such as chromium produce almost as many secondaries as the heavier elements but, because of their lower surface energy, they can be deposited as a uniform and continuous film at thicknesses down to 1nm [12]. Any metal film only a few nanometers thick will, within a few seconds, oxidise on contact with the atmosphere but the layer will subsequently remain mechanically stable provided that the oxide is stoichimetric (as is the case for chromium and titanium) because the after reaching a crticial thickness (typically 2-3nm) the rate of oxygen diffusion to the metal interface will be too small to permit further oxidation. Other metals such as tungsten also have promising

properties as coatings but the oxides that they produce are non-stoichimetric and porous. In this case there is always a finite rate of diffusion to the interface and oxidation can continue indefinitely. Consequently the films are mechanically unstable and tend to deteriorate with time. It would perhaps, in either case, be more precise to speak of 'metal oxide' coatings as being the active agent in the signal production but the basic principles of the signal generation mechanism remain the same.

A thin surface coating also provides a means of circumventing the 'classical' resolution limit discussed above. Monte Carlo calculations [7] show that the yield of SE1 electrons rises very quickly with the thickness of the metal film (figure 10), reaching about 50% of the maximum yield for a thickness of only 1nm to 1.5nm and saturating completely for the thickness of 5nm assumed in figure (7). If a film of 1 to 2nm thickness is deposited uniformly over an object whose size is below the classical limit (figure 11) then as the beam is scanned across the specimen the signal will remain about constant until an edge of the object is reached. At this point the beam sees a projected film thickness which may be several times greater than the average thickness so the SE signal rises. As soon as the beam scans to the top of the edge however the projected film thickness returns to its nominal value and so the signal drops back to its initial value. The total width of the transition will be of the order of the nominal thickness of the film plus the probe size of the beam. The same variation then occurs at the other edge. Thus both edges of the feature are now clearly delineated even though their separation is only a few nm. This 'mass thickness' contrast method is of course only applicable in cases where a sufficiently thin and uniform film can be deposited, and in circumstances where the secondary yield from the film is significantly greater than the yield from the specimen itself. The value of this approach is demonstrated by figure (9b) which shows an image of a similar protein covered sphere to that of figure 9(a) but coated with 2nm of chromium. The improvement in signal to noise ratio is evident, and the improvement in resolution is evidenced by the fact that the protein strings can now be clearly distinguished and visualized over the entire surface area.

The limits discussed above also apply to metals, semiconductors, and ceramics but, because these materials are higher in atomic number and density and so have both a higher yield of secondaries and a smaller secondary escape depth, they only become significant at resolutions which are somewhat beyond the values obtainable with current instrumentation. In practice as illustrated by numerous micrographs, such as the 'lattice fringes' imaged by Kuroda and Komoda [13], the effective resolving power of SE images of such materials is already at the nanometer level. Even leaving aside the 'classical' resolution limit discussed earlier, it has been argued that this level of spatial resolution is unexpected because it implies that, in spite of quantum mechanical considerations, secondary production is a strongly localized event. Assuming that a simple application of the Heisenberg uncertainty principle might be valid in this context [14], the diameter of localization d associated with an inelastic event of energy transfer ΔE (eV) at an electron energy of E_0 (keV) is

$$d = \frac{v\,h}{\Delta E} \approx \frac{66\sqrt{E_0}}{\Delta E}\ \text{nm} \qquad (5)$$

which suggests that at 25keV a typical 4eV secondary is delocalized over some 70nm or more. This is misleading as the relevant energy for the secondary is probably that associated with the initiation of the cascade, typically 50 to 100eV, rather than the escape energy, but even then the delocalization would still be predicted to be 3nm. The fact that plasmons - which are collective oscillations and thus in theory completely delocalized - contribute to secondary electron production might also seem to suggest that, despite the micrograph evidence, secondary images should be limited in resolution to a value closer to ten than to one nm. However, the value of delocalization predicted by equation (5) applies only to the case of small scattering angles corresponding to the minimum momentum transfer and hence the maximum excitation distance [15]. A different criterion for localization must be applied to weakly bound electrons [16] based on the conservation of energy and momentum of the struck electron since in the limit of high overvoltage the momentum transfer is dominated by the need to provide sufficient momentum for the ejected free electron. High momentum transfer would also be involved in the generation of secondaries by plasmons. In both of these cases equation (5) then takes the form [16]

$$d = \frac{h}{\sqrt{2m\,\Delta E}} \approx \frac{0.2}{\sqrt{\Delta E}}\ \text{nm} \qquad (6)$$

which is now independent of the incident electron energy and suggests that for ΔE of 20eV the localization is of the order of 0.05nm. In practice the degree of localization will fall somewhere between the extremes represented by equations (5) and (6), and an energy transfer of 20eV will be localized on average to about 1nm [16], an estimate which is in good agreement with the observed resolution limit of SE images. Finally it must be remembered that it is not only the generation of the secondaries that determines the spatial resolution of the image, but also the subsequent diffusion and escape of the secondaries. Little detailed work on the transport of secondary electrons has been performed and a proper study of this aspect of the process is needed before quantitative predictions can be made.

(2) Backscattered Electron Imaging

(a) Principles

Backscattered electrons are incident electrons which having been scattered through angles in excess of 90 degrees within the specimen emerge through the original beam entrance surface of the specimen. The energy of these electrons lies between 50eV and E_0 the incident energy of the beam and has an average value which is of the order of 0.5 E_0. η the yield of backscattered electrons is a monotonic function of the atomic number Z of the target and varies between about 0.06 for carbon (Z=6) and about 0.5 for uranium (Z=92). Despite the fact that, for most materials and beam energies, the yield of backscattered electrons is at least comparable to the yield of secondaries, backscattered electron imaging has not been as popular a technique because of the difficult of constructing a detector of adequate geometrical efficiency, especially within the confines of an immersion lens, and because of a perception that backscattered images are inherently of low resolution.

Monte Carlo calculations show that backscattering is usually the result of a single high angle (>90 degrees) scattering event within the sample. We can conveniently divide the backscattered

electrons into two groups depending on when this occurs (figure 12). A BS1 electron would be one for which the first elastic scattering interaction it encountered after entering the sample was this high angle event. Since elastic mean free paths at 20-30keV are only of the order of a few tens of nanometers this means that typically such an electron would then leave the surface after only having travelled perhaps 20 to 30 nms within the sample. Assuming the usual Bethe [17] stopping power equation we can estimate that the electron is depositing energy at a rate of from 1 to 10eV per nm of travel in the sample, so it will emerge from the specimen with an energy which is within a few hundred electron volts of E_0. A BS2 electron would be one that encounters its high angle event after undergoing several previous smaller angle events. Because the electron will already have travelled a significant distance in the specimen, the energy of the emergent backscattered electron will now be several keV less than E_0. BS1 electrons can therefore be separated from BS2 electrons by an energy sensitive detector. Since most backscatter detectors exhibit a response which rises linearly with the energy of the electron detected the BS1 electrons will thus be preferentially weighted compared to the BS2 component. Operation at high magnification will, as in the case of secondary imaging, also effectively holds the BS2 component of the signal constant while revealing the spatial variation of the BS1 signal.

BS1 electrons are important for high resolution imaging because the scattering events are highly localized. In order for a high angle event to occur the incident electron must pass very close to the scattering nucleus, for example in silicon at 20keV the impact parameter for backscattering is less than 0.01Å. The probability of this event varies as about Z^2, where Z is the atomic number of the nucleus, thus it is also strongly dependent on the local chemistry of the specimen. Even though the number of BS1 electrons is only a small fraction of the total BS signal (typically from 0.01 to 0.1%) acceptable images may readily be obtained on the right kind of sample. Figure (13) compares secondary and backscattered images (recorded simultaneously) of 10nm colloidal gold particles on a silicon substrate. It is evident that the backscattered image shows both higher resolution and better contrast than the secondary image even though the BS detector used here was not of the energy filtering type. This type of image has already been used in the biological sciences to observe heavy metal labels attached to site specific binding groups on the surfaces of cells and organelles, but recent work [18] has shown that when utilised in conjunction with heavy metal

shadowing techniques it can also reveal structural detail on biological crystals at the sub-nanometer level. BS1 imaging is related to the 'low-loss' mode originally described by Wells [19], and can be considered as an extreme example of the high angle annular dark field STEM mode [20] but with the notable advantage of being feasible from a solid sample.

(b) Information in the BS image

The intensity of the backscatter signal depends on the mean atomic number of the target, but since the backscattered electrons sample a volume of the sample comparable in diameter to the Bethe range (equation 3), the actual magnitude of the effective backscattering coefficient observed from an inhomogeneous specimen will represent an average over the entire sampled volume. With the exception of the BS1 component, therefore, the spatial resolution of the image will be a function of the Bethe range and so only capable of 'high resolution' at low beam energies. Unlike the secondary signal which is generated at or close to the surface of the specimen the backscatter signal carries information from depths of up to one-third of the Bethe range within the sample, so in general it is less surface specific. At low beam energies (< 2keV) however the depth of information of the backscatter signal may become less than the escape depth of the secondary electrons. In this event it is the BS signal which will best display the surface. Backscattered images also contain topographic contrast, i.e a variation in the yield as a function of the local orientation of the surface to the beam, but because backscatter electrons are high in energy compared to secondaries they travel in straight lines and are thus prone to shadowing by surface asperities. BS images of a surface are therefore dependent on the position of the detector relative to the surface.

Electron channeling contrast is also present in BS images from crystalline specimens [21]. In this case the signal depends on the orientation of the beam relative to the lattice so variations of this angle, produced either by an angular displacement of the beam or by local changes in the crystallography of the sample, will produce contrast. Figure (14) shows contrast imaged from edge dislocations in a bulk sample of molybdenite using this method after setting the specimen to a carefully chosen orientation relative to the incident beam by means of a selected area channeling pattern [22]. The spatial resolution in this case is determined both by the extent of the bending of

lattice planes around the dislocations and by the angular convergence of the beam rather than by any limitation set by the size of the probe itself. Because the required electron-optical conditions are restrictive, and the contrast is only 3-4% at maximum, this form of imaging is only possible on a FEG instrument.

Applications of the high resolution SEM

It can be estimated that there are only about 150 high resolution SEMs installed worldwide, and of these all but 20 or so are in Japan. While these instruments have been employed on a wide range of problems only a small fraction of the work has yet been published in the open literature. The major areas of application in the physical sciences have been to the study of surfaces, for example observations of wear on high density magnetic recording media [23] and studies on the mechanisms of crystal growth, observations of semiconductors [24] including such areas as layered structures and quantum wells, and studies of polymers and composites. In the life sciences studies include the observation of cellular ultra-structure [25], the direct visualization of macro-molecular structures [26], and studies of the morphology of tooth enamel [27]. As more of these instruments become available the number and variety of the applications described will undoubtedly increase.

Conclusions

The combination of a field emission gun and a high performance probe-forming lens produces a scanning electron microscope that combines much of the convenience and appeal of a conventional SEM with a spatial resolution that can rival that of the transmission electron microscope. Although much theoretical and practical work remains to be done to place this technique on a firm footing, it is already clear that this new generation of SEMs can make a major contribution to both the physical and life-sciences.

Acknowledgements The author is grateful to Dr.S J Pennycook for helpful comments and clarifications on the question of the localization of secondary electron generation.

References

[1] Kimura H and Tamura H, 1967, New method of detecting Secondary Electrons on Scanning Electron Microscope, Proc. 9th Ann.IEEE Symp. on Electron, Ion and Laser Beams, 198-205

[2] Goldstein JI, Newbury DE, Joy DC, Echlin PE and Lifhsin E, 1981, Introduction to Scanning Electron Microscopy and Xray Microanalysis, (Plenum Press:NY)

[3] Cliff G and Kenway P, 1983, Optics of Probe forming lens, in Electron Microscopy and Microanalysis 1983, ed P J Doig, (Inst. of Physics:Bristol), IP Conf. Ser. **68**, 83-86

[4] Dodson T A and Joy DC, 1990, Measurement of Resolution SEM by Fourier Transform methods, Proc. XIIth Int. Congr. on Electron Microscopy, Seattle, (in press)

[5] Seiler R, 1982, Secondary Electrons in the SEM, J.Appl.Phys.**54**, R1-R18

[6] Drescher H, Reimer L and Seidel H, 1970, Ruckstreukoeffizient und Sekundarelektronen Ausbeute von 10-100keV, Z. Agnew Phys. **29**, 331-336

[7] Joy D C, 1984, Monte Carlo studies of High Resolution Imaging, in Microbeam Analysis 1984, ed A Romig and J I Goldstein, (San Francisco Press:San Francisco), 81-86

[8] Luo S and Joy DC, 1988, Monte Carlo calculations of secondary electron emission, Scanning Microscopy **2**, 1901-1916

[9] Liu J, 1989, Ultra-high resolution secondary electron imaging, Proc. 47th Ann.Meeting EMSA, ed G W Bailey, (San Francisco Press:San Francisco), 66-67

[10] Joy DC, 1989, Image Simulation for High Resolution Scanning Electron Microscopy, in Computer Simulation of EM Diffraction and Images, ed W Krakow and M O'Keefe, (Minerals,

Metals and Materials Society:Warrendale, PA), 209-220

[11] Joy DC, 1984, Beam Interactions, Contrast and Resolution in the SEM, J.of Micros. **136**, 241-248

[12] Peters K-R, 1985, Working at Higher Magnifications in SEM, Scanning Electron Microscopy, **IV**, 1519-1544

[13] Kuroda T and Komoda T, 1985, Observations of W-<110> surface in SEM, J.Electron.Micros. **34**, 179-182

[14] Craven AJ, Gibson JM, Howie A and Spalding DR, 1978, Study of single electron excitations by electron microscopy-(1) Image Contrast from delocalized excitations Phil.Mag. **A 38**, 519-527

[15] Pennycook SJ and Howie A, 1980, Study of Single-Electron excitations by Electron Microscopy II. Cathodoluminescence image contrast from localized energy transfers, Phil.Mag., **41**, 809-827

[16] Pennycook SJ, 1988, Delocalization Corrections for Electron Channeling Analysis, Ultramicroscopy **26**, 239-248

[17] Bethe H, 1930, Theory of passage of swift corpuscular rays through matter, Ann.Phys. **5**, 235-243

[18] Gross H et al, 1990, Proceedings 4th Int. Conf. on Low Temperature Microscopy and Microanalysis, (Cambridge, April 1990), to be published in The Journal of Microscopy.

[19] Wells OC, 1971, Low Loss Image for Surface SEM, Appl.Phys.Lett., **19**, 232-235

[20] Pennycook S and Jesson DA, 1990, High Resolution Incoherent Imaging of Crystals, Phys.Rev.Lett.,**64**, 938-941

[21] Joy DC, Newbury DE, and Davidson D L, 1982, Electron Channeling Patterns in the SEM, J.Appl. Phys. **53**, R81-R132

[22] Joy DC, 1990, Direct Imaging of Defects in High Resolution SEM, in 'High Resolution Electron Microscopy of Defects in Materials", ed R Sinclair, D J Smith and U Dahmen, (Materials Research Society:Pittsburgh, PA), MRS Symposium Proc., **183**, 199-210

[23] Chan L, Yamashita T and Sinclair R, 1989, TEM and high resolution SEM of Co-Ni-Pt thin film magnetic recording media, Proc. 47th Ann.Meeting EMSA, ed G W Bailey, (San Francisco Press:San Francisco), 570-571

[24] Krause SJ, Maracas GN, Varhue WJ and Joy DC, 1989, High Resolution SEM of semiconductors, Proc. 47th Ann.Meeting EMSA, ed G W Bailey, (San Francisco Press:San Francisco), 82-83

[25] Apkarian AP, 1989, SE-1 imaging of chromium coated biological specimens, Proc.47th Ann.Meeting EMSA, ed G W Bailey, (San Francisco Press:San Francisco), 68-69

[26] Peters K-R, 1988, Ultra-high resolution SEM at high voltage images of individual *fab* fragments applied as a molecular label to cell surface receptors, Proc.47th Ann.Meeting EMSA, ed G W Bailey, (San Francisco Press:San Francisco), 70-71

[27] Apkarian AP, Gutekunst MD, and Joy DC, 1990, High Resolution SE-1 SEM study of Enamel Crystal Morphology, J.Elect.Micros.Techn.,**14**, 70-78

Figure Captions

(1) The variation of incident beam current with probe size for (a) a conventional SEM with a tungsten hairpin thermionic emitter and a pinhole-lens (C_s = 2cm, β = 10^5 amps/cm^2/str), (b) an SEM with conventional optics but using a field emission gun (C_s = 2cm, β = 10^8 amps/cm^2/str), and (c) a high performance SEM with both a field emission gun and an immersion lens (C_s = 2mm, β = 10^9 amps/cm^2/str).

(2) Ray tracing simulations, based on the method of Cliff and Kenway [3], of probe forming and current profiles in SEMs at 30keV and 2keV using identical lenses but either a cold field emission gun, or a LaB_6 thermionic emitter.

(3) The origin of the SE1 and SE2 components of the secondary signal.

(4) Schematic view of the emission profile of secondary electrons from a surface.

(5) High resolution secondary electron image of an anodized alumina inorganic membrane. Image recorded at 25keV on an Hitachi S-900.

(6) High resolution image of a layered Si and Ge structure on silicon. Imaged at 3keV in Hitachi S-900.

(7) Monte Carlo calculation of yield of SE1 electrons from top 5nm region of selected elements at 20keV.

(8) Origin of the classical limit to the spatial resolution of secondary electron imaging in the SEM.

(9) Secondary electron images of monoclonal anti-body protein bound to a polystyrene sphere (a) with no surface coating and (b) with 2nm of chromium. Images recorded at 25keV in Hitachi S-900.

(10) Monte Carlo calculation of yield of SE1 electrons from chromium versus thickness of film for 20keV beam energy.

(11) Illustration of the use of SE1 mass-thickness contrast to image structures with a size below the classical resolution limit.

(12) The origin of BS1 and BS2 backscatter electron components.

(13) Secondary electron (a) and backscattered electron (b) images of 10nm colloidal gold particles on a silicon substrate. Images acquired simultaneously at 20keV on Hitachi S-900.

(14) Channeling contrast image of edge dislocations in a bulk foil of molybdenite, imaged in a <2020> reflection. Micrograph recorded in backscatter mode at 25keV in Hitachi S-900.

DISCLAIMER

This report was prepared as an account of work sponsored by an agency of the United States Government. Neither the United States Government nor any agency thereof, nor any of their employees, makes any warranty, express or implied, or assumes any legal liability or responsibility for the accuracy, completeness, or usefulness of any information, apparatus, product, or process disclosed, or represents that its use would not infringe privately owned rights. Reference herein to any specific commercial product, process, or service by trade name, trademark, manufacturer, or otherwise does not necessarily constitute or imply its endorsement, recommendation, or favoring by the United States Government or any agency thereof. The views and opinions of authors expressed herein do not necessarily state or reflect those of the United States Government or any agency thereof.

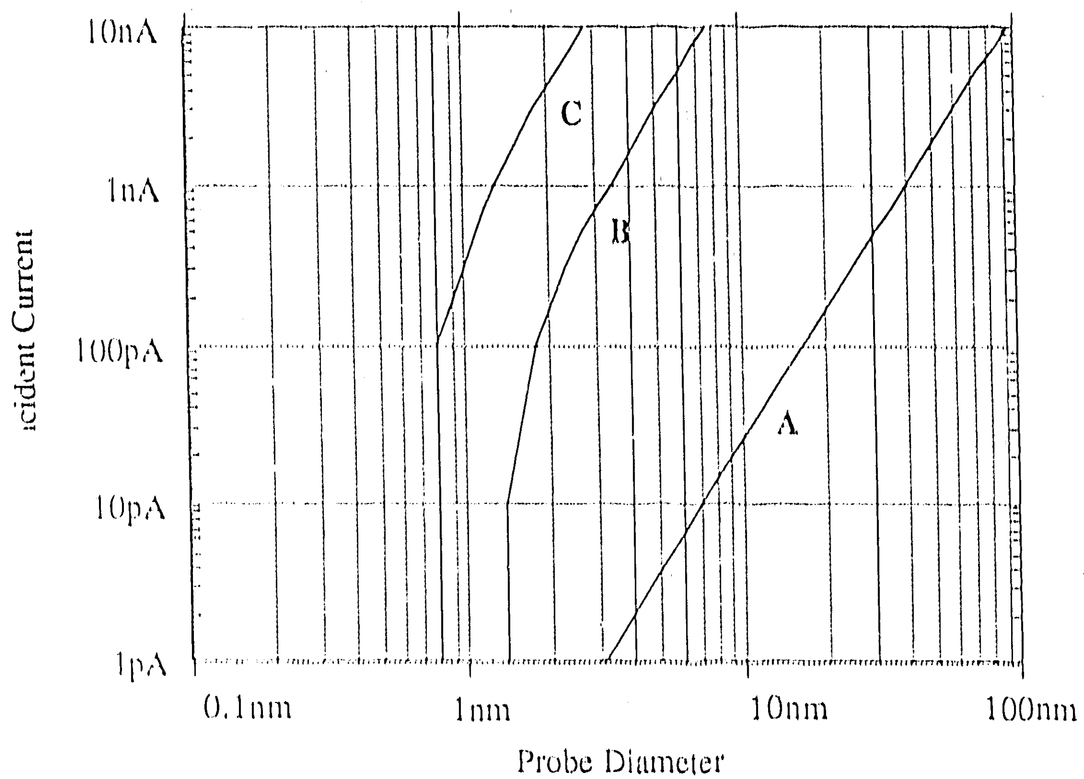

Figure (1) The variation of incident beam current with probe size for (A) a conventional SEM with a tungsten hairpin thermionic emitter and a pinhole-lens (C_s = 2cm, β = 10^5 amps/cm²/str), (B) an SEM with conventional optics but using a field emission gun (C_s = 2cm, β = 10^8 amps/cm²/str), and (C) a high performance SEM with both a field emission gun and an immersion lens (C_s = 2mm, β = 10^9 amps/cm²/str).

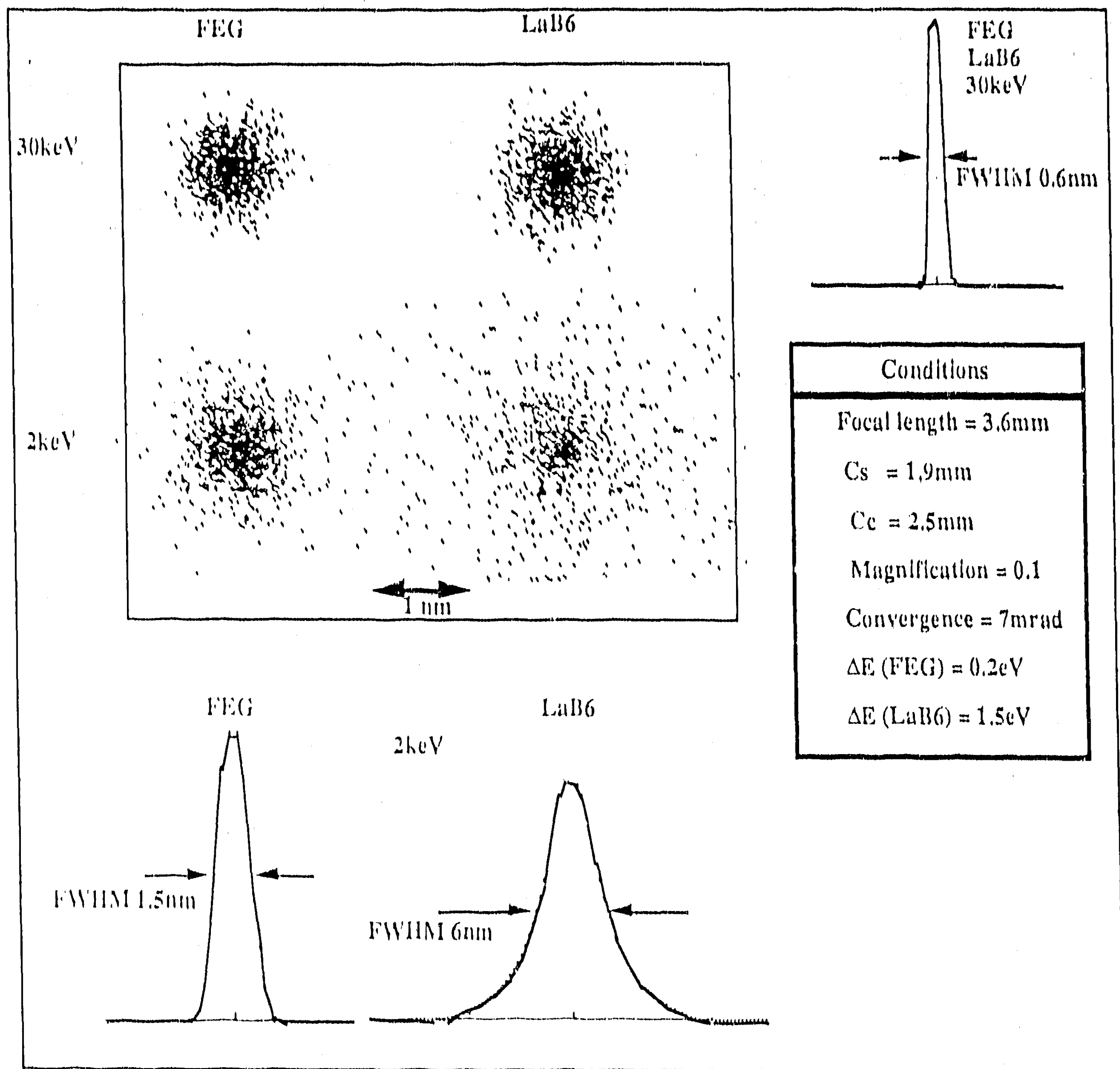

Figure (2) Ray tracing simulations, based on the method of Cliff and Kenway [3], of probe forming and current profiles in SEMs at 30keV and 2keV using identical lenses but either a cold field emission gun, or a LaB_6 thermionic emitter.

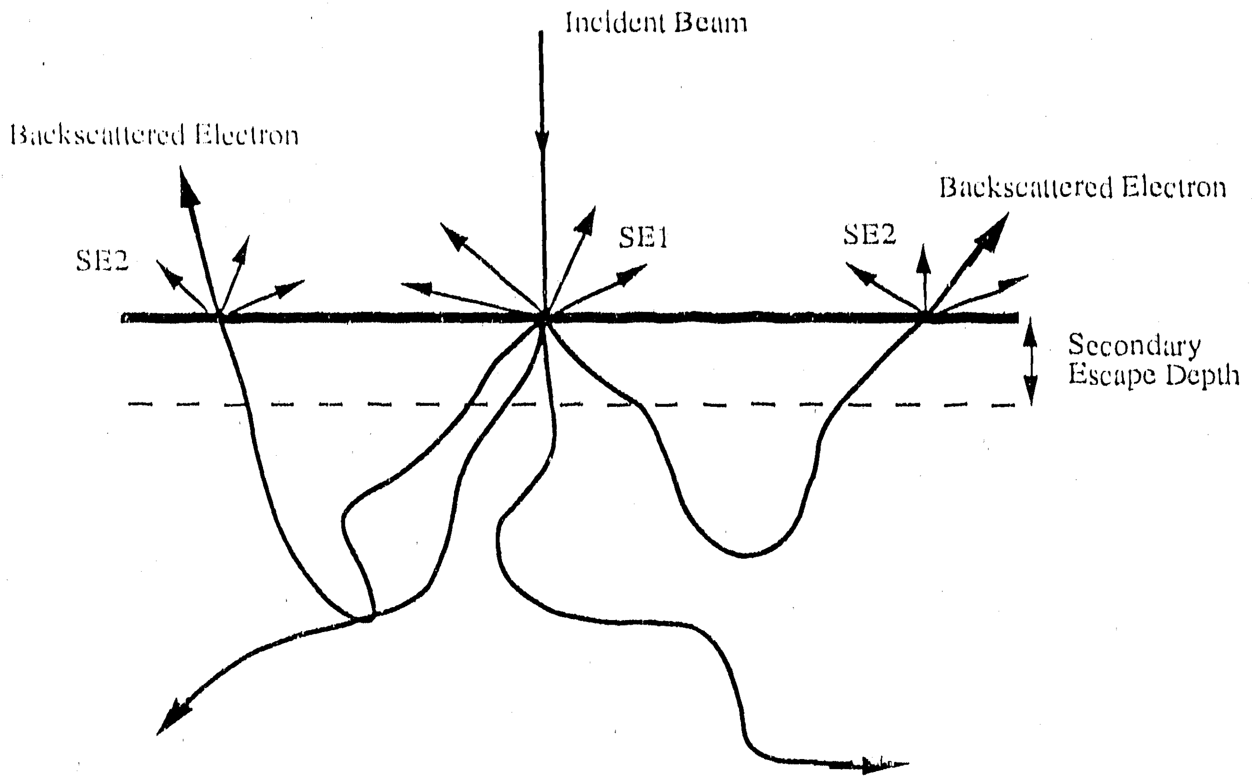

Figure (3) The origin of the SE1 and SE2 components of the secondary signal.

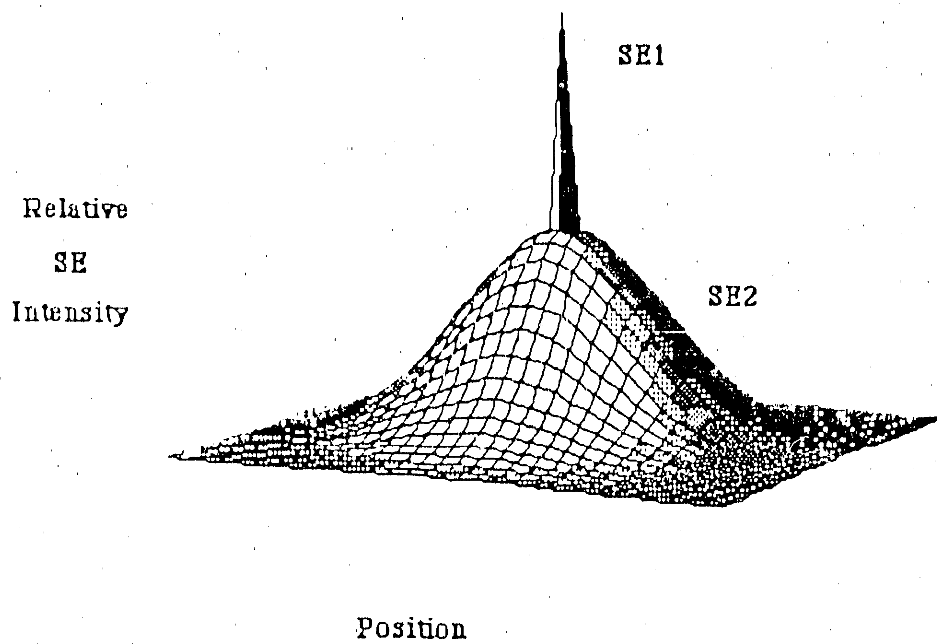

Figure (4) Schematic view of the emission profile of secondary electrons from a surface.

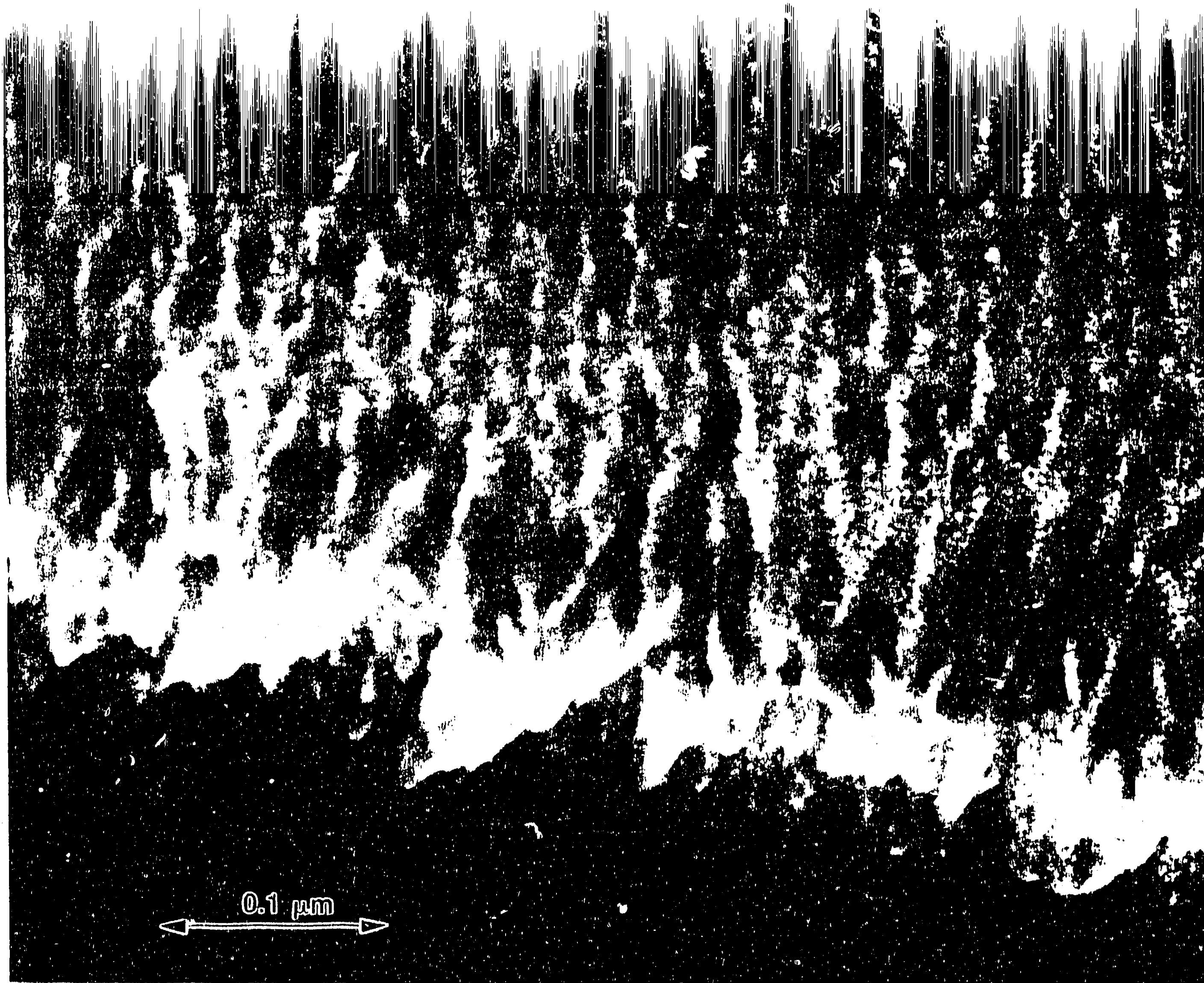

(5) High resolution secondary electron image of an anodized alumina inorganic membrane. Image recorded at 25keV on an Hitachi S-900.

(6) High resolution image of a layered Si and Ge structure on silicon. Imaged at 3keV in Hitachi S-900.

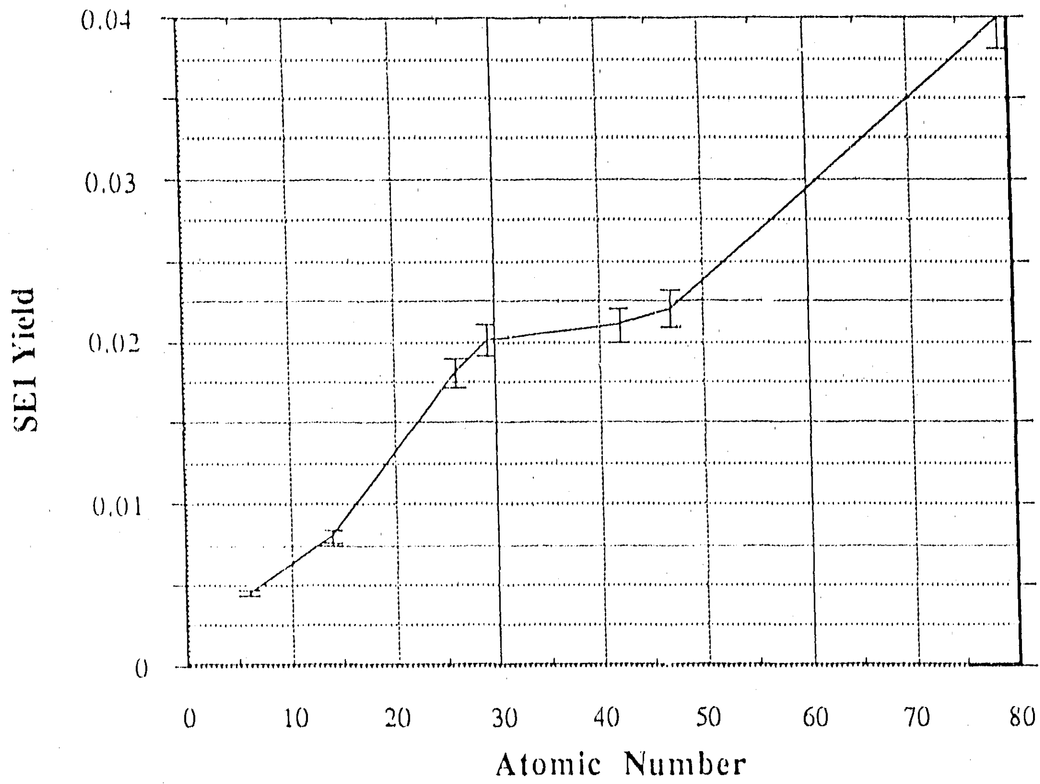

Figure (7) Monte Carlo calculation of yield of SE1 electrons from top 5nm region of selected elements at 20keV beam energy.

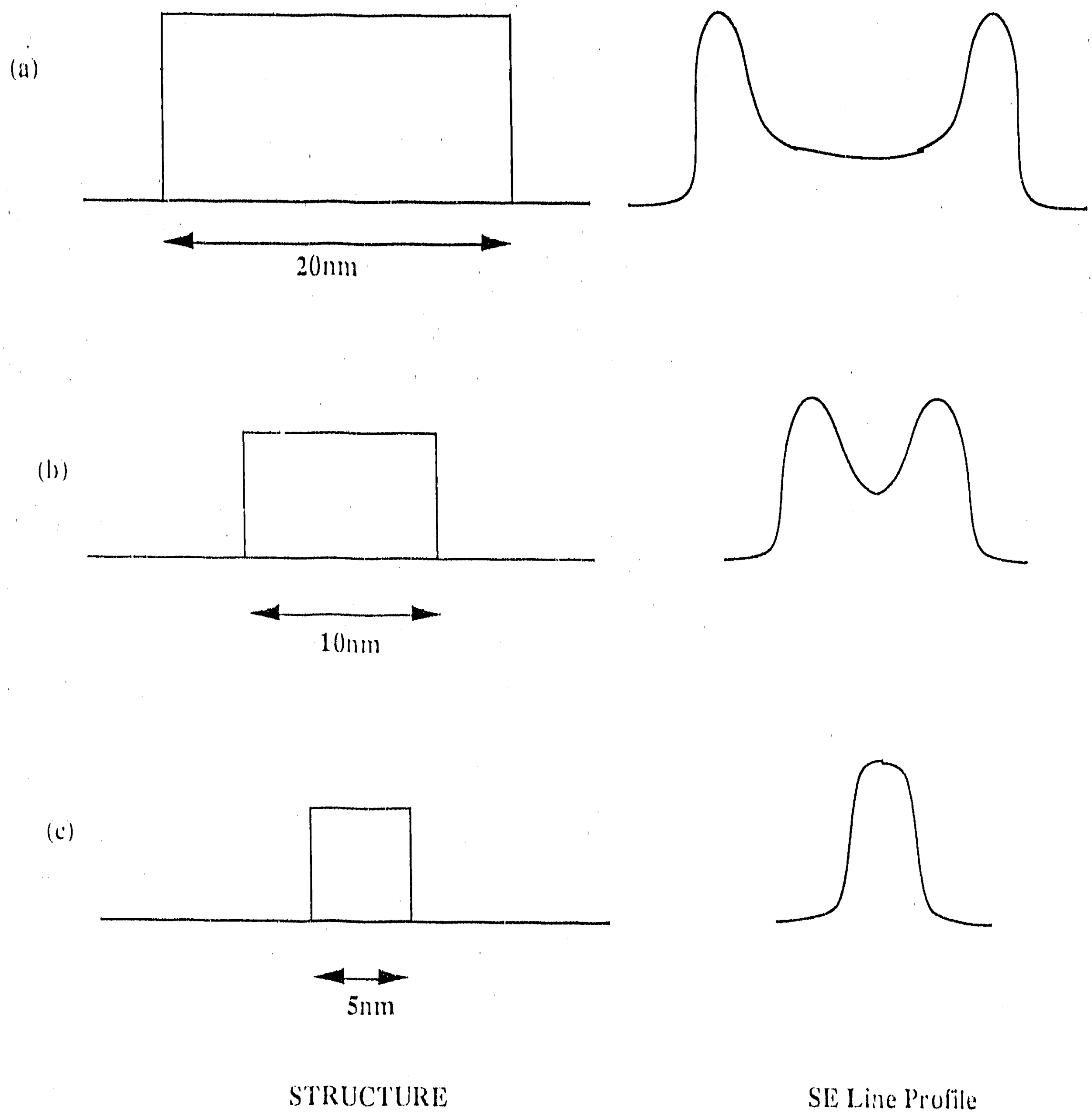

Figure (8) Origin of the classical limit to the spatial resolution of secondary electron imaging in the SEM.

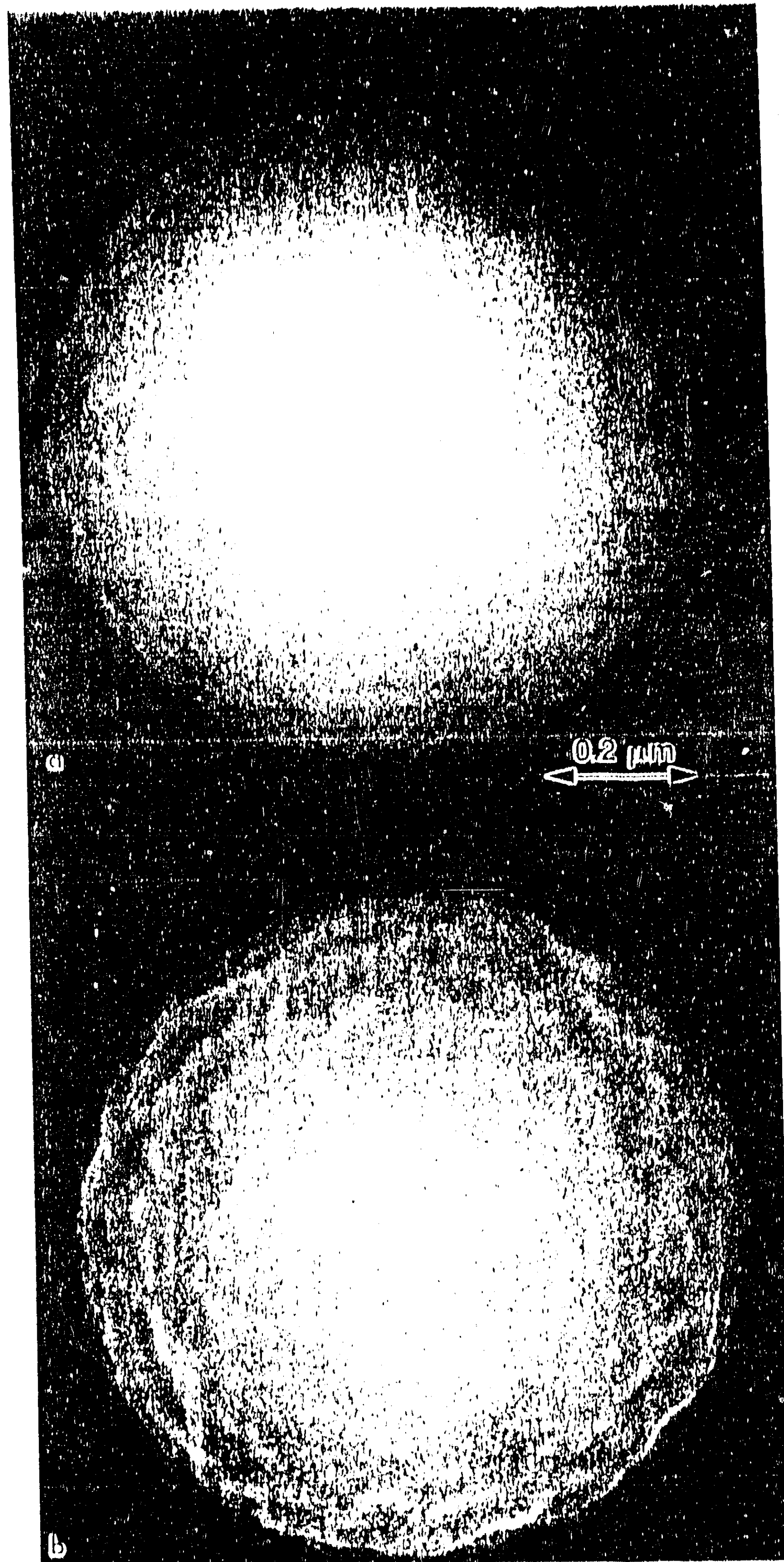

(9) Secondary electron images of monoclonal anti-body protein bound to a polystyrene sphere (a) with no surface coating and (b) with 2nm of chromium. Images recorded at 25keV in Hitachi S 900.

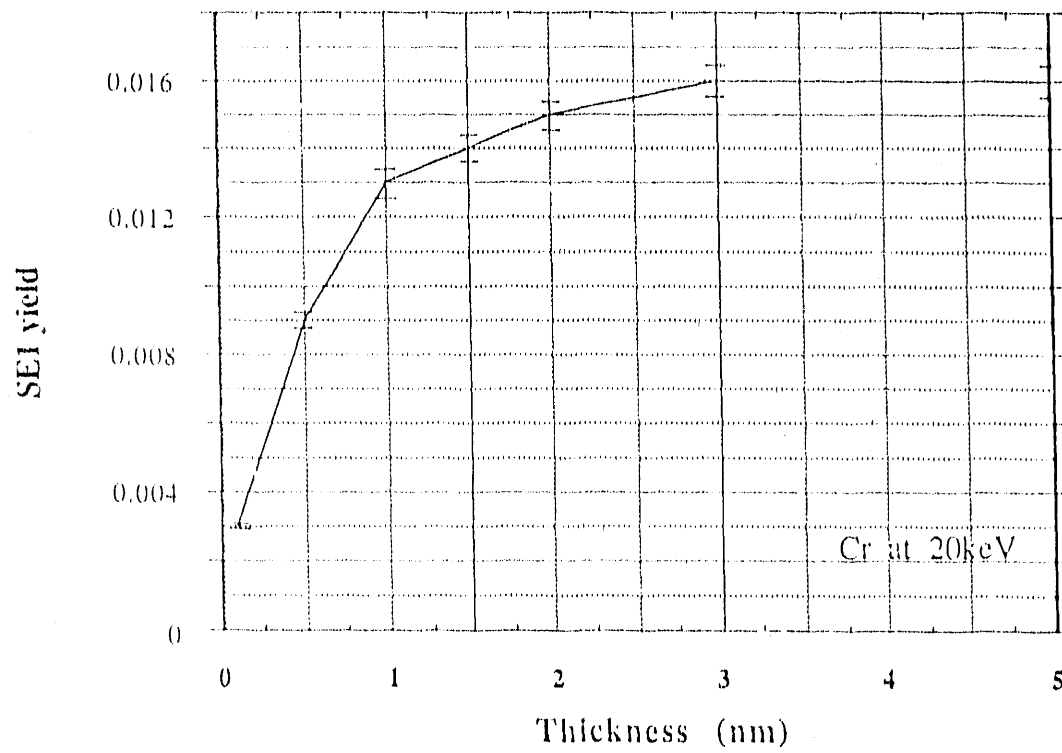

Figure (10) Monte Carlo calculation of yield of SE1 electrons from chromium versus thickness of film, for 20keV beam energy.

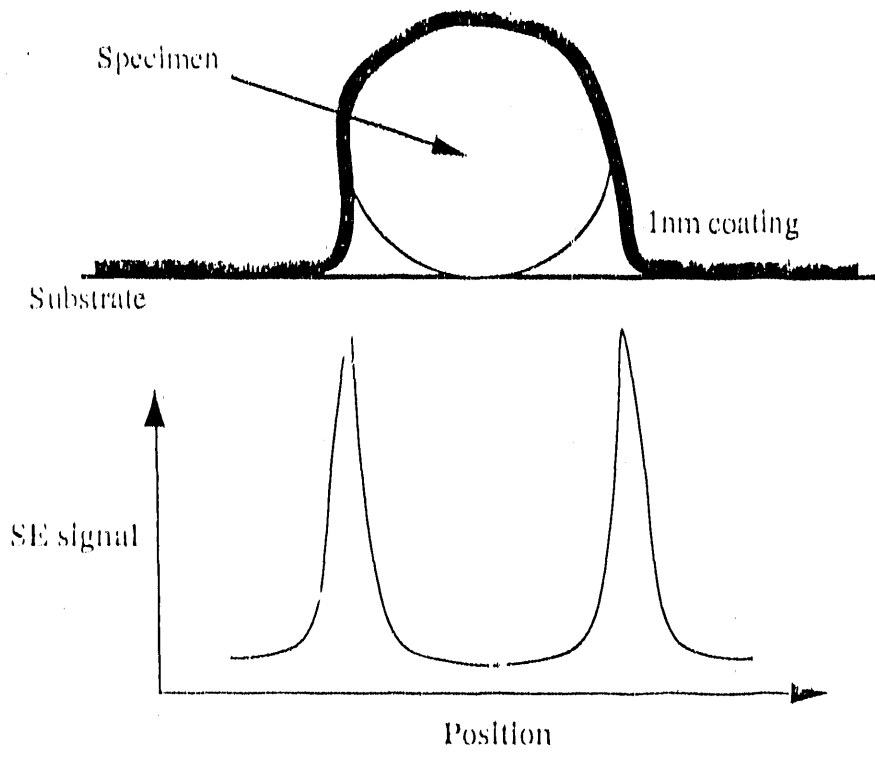

Figure (11) Illustration of the use of SE1 mass-thickness contrast to image structures with a size below the classical resolution limit.

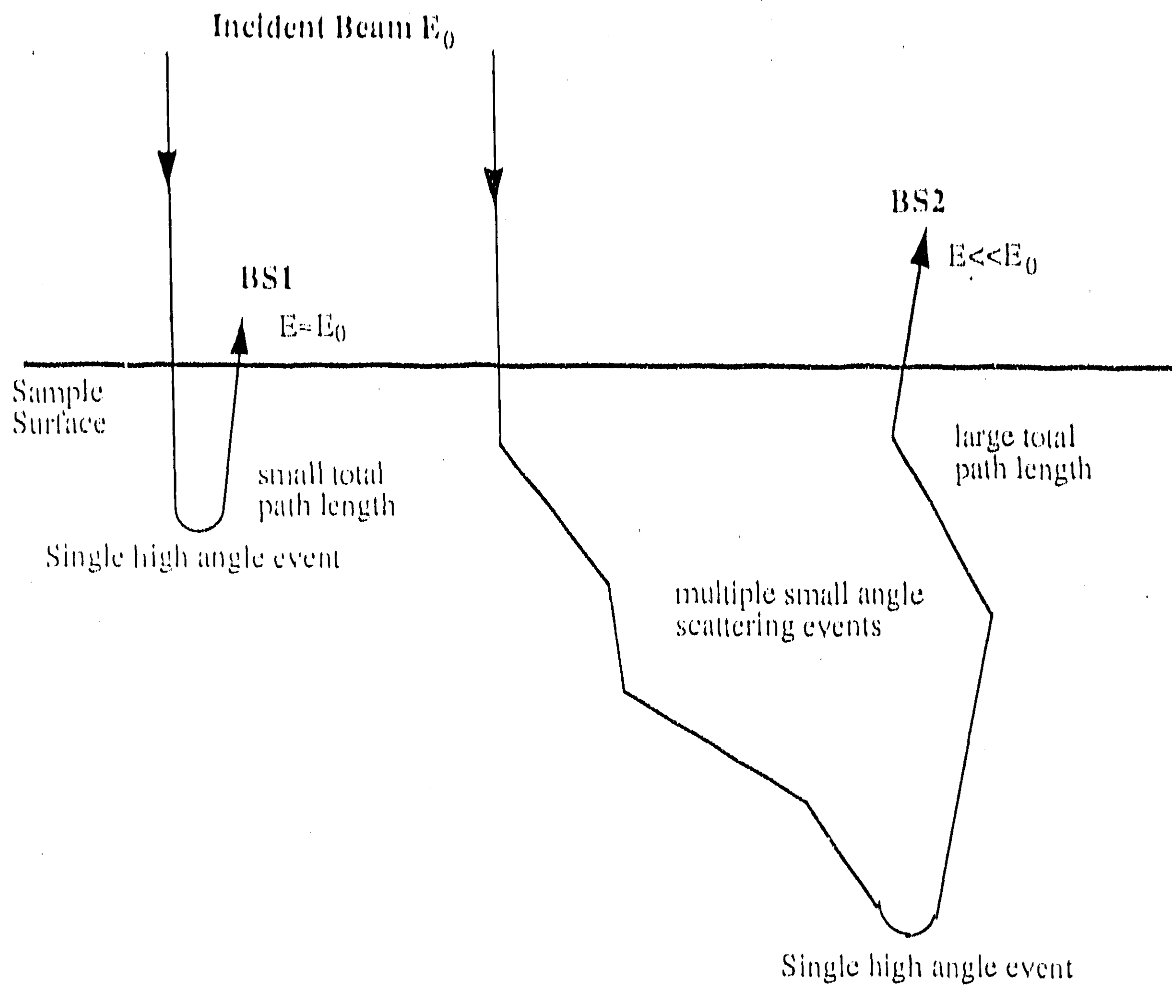

Figure (12) The origin of the BS1 and BS2 backscatter electron components.

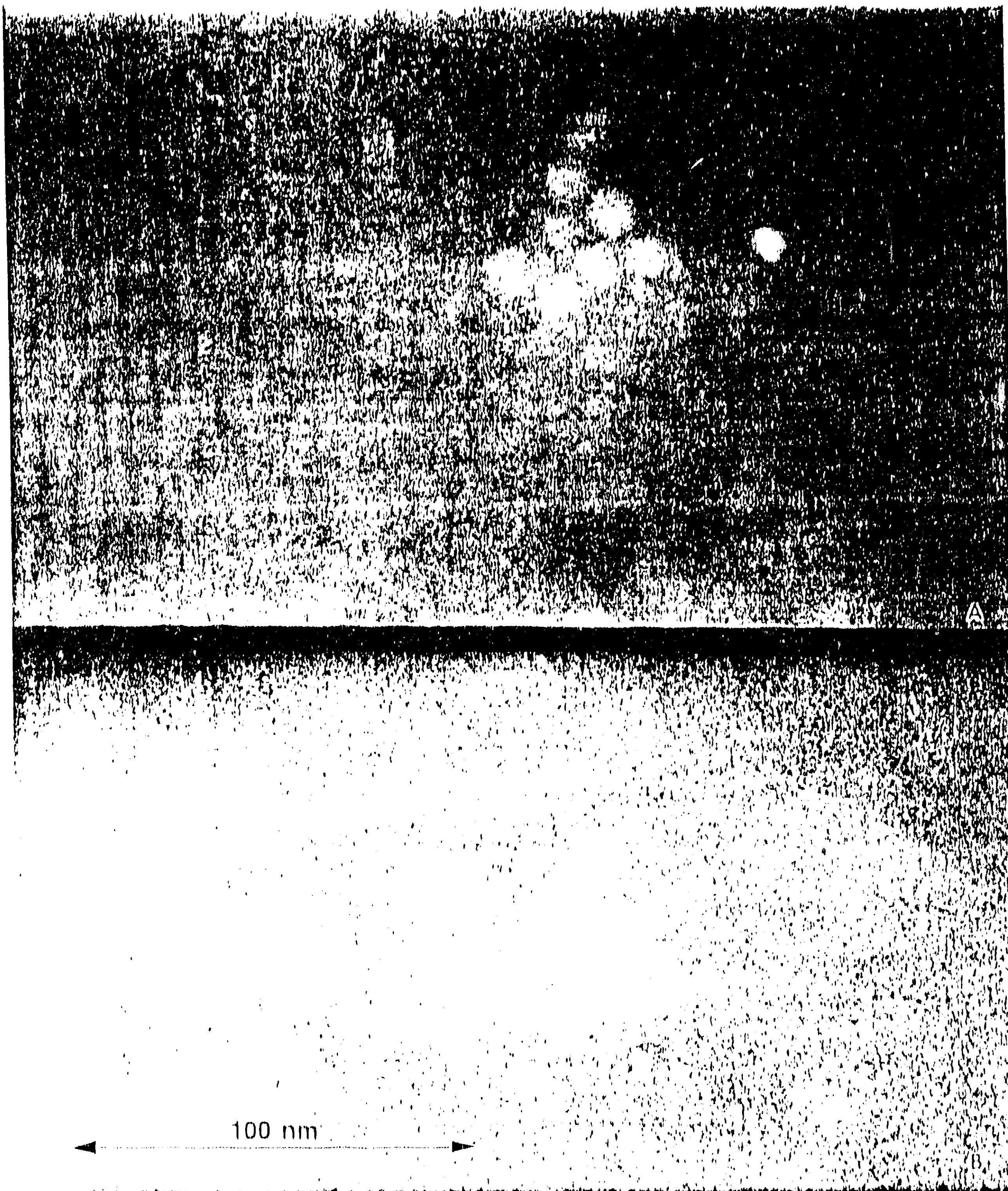

(13) Secondary electron (a) and backscattered electron (b) images of 10nm colloidal gold particles on a silicon substrate. Images acquired simultaneously at 20keV on Hitachi S-900.

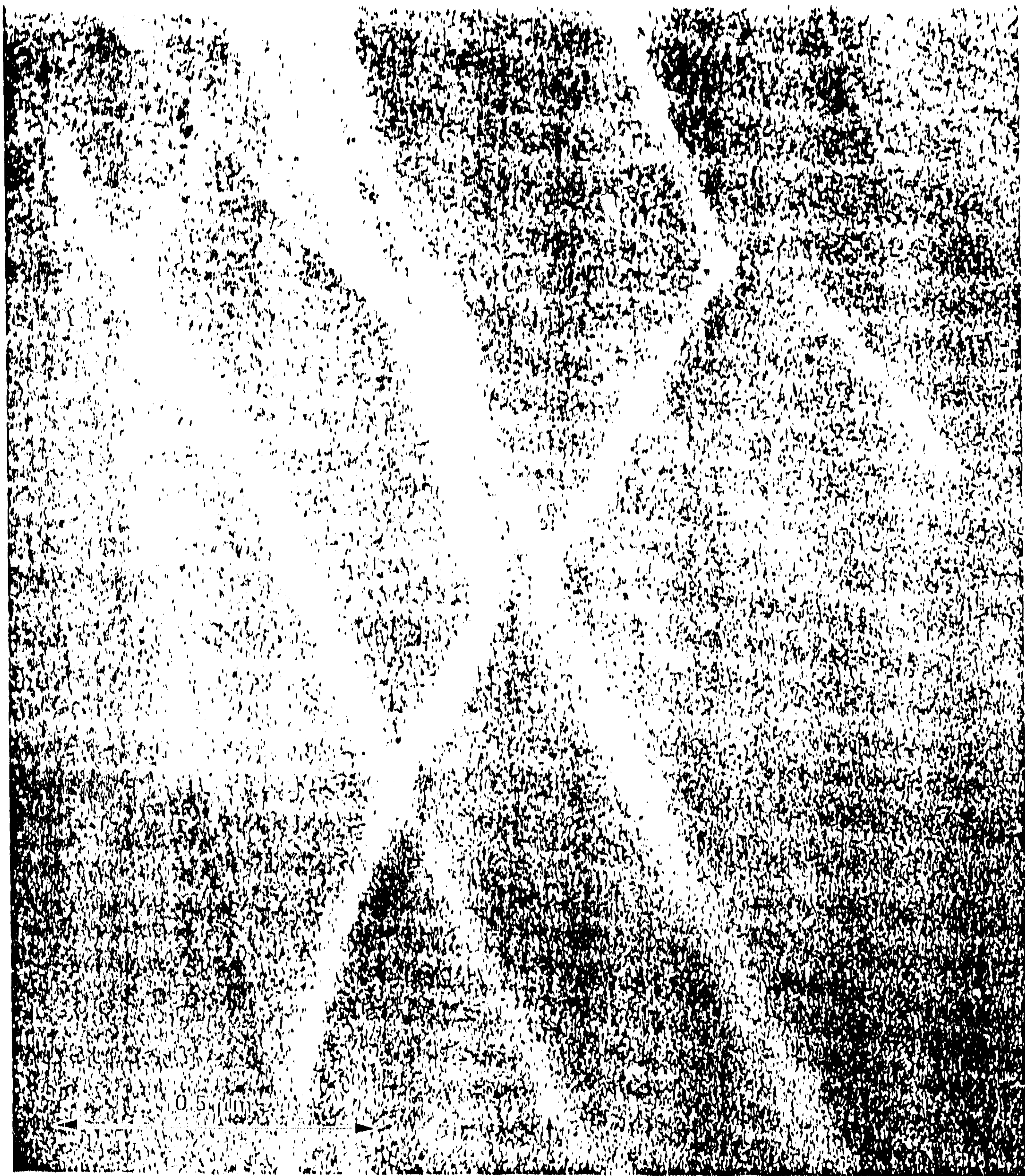

(14) Channeling contrast image of edge dislocations in a bulk foil of molybdenite, imaged in a <2020> reflection. Micrograph recorded in backscatter mode at 25keV in Hitachi S-900.

- END -

DATE FILMED

11 / 1 / 90